JASMAC Conference of the Japan Society of Microgravity Application

PS16

フェーズフィールド LBM とゴーストノード法のカップリングによる液滴衝突解析

Numerical study of binary droplets collision using coupling the phase-field lattice Boltzmann method and the ghost node method.

濵田 航汰, 田川 俊夫
Kota HAMADA, Toshio TAGAWA
東京都立大学　大学院院システムデザイン研究科　航空宇宙システム工学域,
Department of Aeronautics and Astronautics, Tokyo Metropolitan University

1. Introduction

1.1. Background

Computational fluid dynamics is a field that uses computers to solve and analyze approximately the Equation of continuity and Navier-Stokes equations. This field has developed with the improvement of computer performance and has advantages, such as easier parameter settings and the ability to simulate environments where experiments are difficult to perform. In addition, various methods have been developed to date, and these methods have the advantage capable to analyze and consider multiple approaches depending on the system being simulated. On the other hand, it is rare for simulation results to completely match experimental results, and it is important to know how to evaluate differences.

Currently, the analysis of fluid phenomena is used in many places, and it is an important issue that is related to the fuel efficiency of automobiles and airplanes, as well as the power generation performance of hydroelectric and wind power plants. Among them, gas-liquid two-phase flow is a fluid motion in which gas and liquid coexists, and it has a great impact on the core parts of systems such as inside engines and nuclear power plants. In particular, droplet collision problems affect the formation of raindrops and spray coatings, and the head-on collision between droplets, which is the subject of this study, plays an important role in the spray phenomenon and drug protection. There are various collision forms depending on the Weber number (We), the collision parameter (I), and the species of liquid [1].

$$We = \frac{\rho_h D U_0^2}{\sigma} \tag{1}$$

$$I = \frac{b}{D} \tag{2}$$

Brazier-Smith [2] conducted experiments on droplet collisions. Subsequently, Ashgriz and Poo [1] conducted droplet collision experiments with the same and different sizes and concluded that collision dynamics can be classified by the Weber number, collision parameters, and droplet size ratio. Here, the Weber number represents the ratio of inertial force to surface tension, and the collision parameters represent the eccentricity of the droplet in the collision direction. Various models have been proposed for numerical analysis, including the study of Nikolopoulos and Bergeles [3] using the VOF method and the study of Pan and Suga [4] using the level set method.

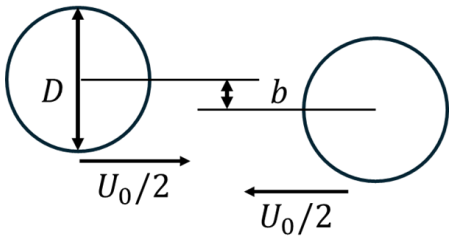

Figure 1. Model of droplet collision.

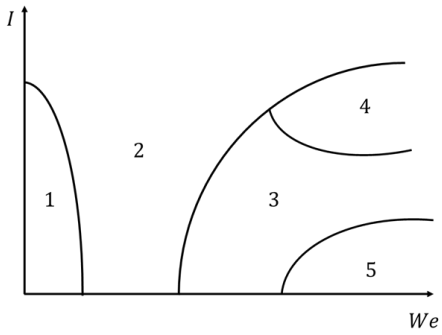

Figure 2. *We-I* diagram collision outcome regimes, 1. SPC (soft permanent-coalescence): coalescence after minor deformation, 2. B: Bouncing of the droplets, 3. HPC (hard permanent-coalescence): coalescence after substantial deformation, 4. CFRS (coalescence followed by reflexive separation): coalescence followed by separation for near head-on collisions, 5. CFSS (coalescence followed by stretching separation): coalescence followed by separation for off-center collisions.

As can be seen from the above, simulations have been performed using a variety of methods, but there are still some issues such as instability of the droplet interface, mass conservation, and instability due to large density ratios. In addition, many methods currently used are not suitable for parallel calculation, and there are high hurdles to high-speed calculations. Furthermore, when trying to solve these problems, models often become complicated, and calculation costs are high. Thus, methods to solve these problems are required.

1.2. Purpose

Based on the above background, the purpose of this study is to perform numerical analysis using the proposed method on collision phenomena related to head-on collisions of droplets, and to verify its validity. The proposed method is a combination of the phase-field lattice Boltzmann method, which is suitable for parallel computing, and the ghost node method, which has a low implementation cost.

2. Numerical Method

2.1. Calculation model

The calculation model used in this study is shown in Fig. 3. The characteristic length is the droplet diameter, the characteristic velocity is the initial velocity, and the effect of gravity is ignored. The calculation area is $2 \times 2 \times 4$, where the droplet diameter is 1. In addition, because this study calculates a head-on collision, the impact parameter (I) is set to 0.

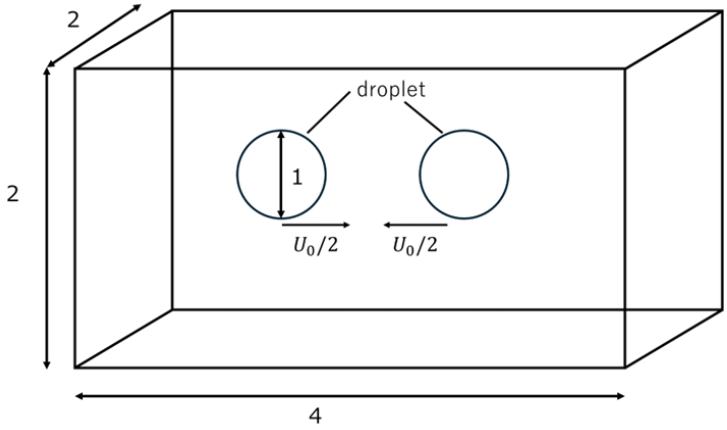

Figure 3. Calculation model.

2.2. Phase-field lattice Boltzmann method

2.2.1. Macroscopic equation

The interface capturing method employs the phase-field method. The phase-field method assumes a certain width at the interface and solves the conservative Allen-Chan equation [5] for the order parameter ϕ. Using this method, it is possible to calculate complex interface shapes and surface tensions. The order parameter ϕ is expressed as follows:

$$\phi = \frac{1}{2}(1 + \tanh\frac{2s}{W}) \tag{3}$$

Where W is the interface width, s is the signed distance from the interface. $\phi = 0$ is the gas phase side, $\phi = 1$ is the liquid-phase side. The model is shown below.

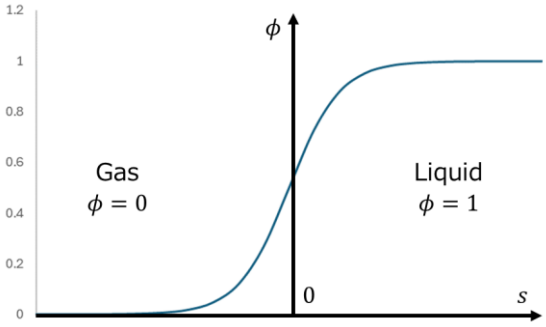

Figure 4. Transition of order parameter (ϕ).

We solve the Conservative Allen-Chan equation.

$$\frac{\partial\phi}{\partial t} + \frac{\partial\phi u_\alpha}{\partial x_\alpha} = \frac{\partial}{\partial x_\alpha} M\left[\frac{\partial\phi}{\partial x_\alpha} - n_\alpha\left[\frac{1-4(\phi-\phi_{ave})^2}{W}\right]\right] \tag{4}$$

Where M is the mobility, ϕ_{ave} is the arithmetic mean of the gas and liquid phases, which is set to 0.5 in this study, and n_α is the unit normal vector of the interface, which is expressed by the following formula.

$$n_\alpha = \frac{\partial\phi}{\partial x_\alpha} \Big/ \left|\frac{\partial\phi}{\partial x_\beta}\right| \tag{5}$$

Equation of continuity and Navier-Stokes equation are as follows:

$$\frac{\partial u_\alpha}{\partial x_\alpha} = 0 \tag{6}$$

$$\rho\left(\frac{\partial u_\alpha}{\partial t}+u_\beta\frac{\partial u_\alpha}{\partial x_\beta}\right)=-\frac{\partial p}{\partial x_\alpha}+\frac{\partial}{\partial x_\beta}\left[\mu\left(\frac{\partial u_\alpha}{\partial x_\beta}+\frac{\partial u_\beta}{\partial x_\alpha}\right)\right]+F_\alpha^s+F_\alpha^b \tag{7}$$

Where ρ is the density, μ is the viscosity.

$$\rho=\rho_l+\phi(\rho_h-\rho_l) \tag{8}$$

$$\mu=\mu_l+\phi(\mu_h-\mu_l) \tag{9}$$

The subscript h means high and l means low. F_α^s is a surface tension term and F_α^b is a gravity term, which are defined by the following formula.

$$F_\alpha^s=\eta\frac{\partial\phi}{\partial x_\alpha} \tag{10}$$

$$F_\alpha^b=-\rho g_\alpha \tag{11}$$

η is the chemical potential and is defined as follows:

$$\eta=4\beta\phi(\phi-1)(\phi-\phi_{ave})-\kappa\frac{\partial^2\phi}{\partial x_\alpha\partial x_\alpha} \tag{12}$$

$$\beta=\frac{12\sigma}{W} \tag{13}$$

$$\kappa=\frac{3\sigma W}{2} \tag{14}$$

To avoid numerical instability, the pressure is calculated from the pressure equation instead of the state equation. The pressure equation is given by the following formula [6].

$$\frac{\partial p}{\partial t}+\rho c_s^2\frac{\partial u_\alpha}{\partial x_\alpha}=0 \tag{15}$$

2.2.2. Discretization

The conservative Allen-Chan equation is discretized using a weighted MRT model. The distribution function h_i for the order parameter is calculated as follows. We employ the D3Q27 model.

$$h_i(x_\alpha+c_{i\alpha}\delta_t,t+\delta_t)=h_i(x_\alpha,t)-\boldsymbol{M^{-1}S_hM}\ (h_i(x_\alpha,t)-h_i^{eq}(x_\alpha,t)) \tag{16}$$

Where h_i^{eq} is the equilibrium distribution function, and in the phase-field method it is given as follows:

$$h_i^{eq}=\phi w_i\left[1+\frac{c_{i\alpha}u_\alpha}{c_s^2}+\frac{(c_{i\alpha}u_\alpha)^2}{2c_s^4}-\frac{u_\alpha^2}{2c_s^2}\right]+M\left[\frac{1-4(\phi-\phi_{ave})^2}{W}\right]\frac{w_i c_{i\alpha}}{c_s^2}n_\alpha \tag{17}$$

Where c_i is the particle velocity and w_i is the weighting coefficient. The D3Q27 model used in this analysis is described as follows:

Table 1. Particle velocity.

$\boldsymbol{i}$	c_i	w_i
0	(0,0,0)	8/27
1~6	$(\pm1,0,0),(0,\pm1,0),(0,0,\pm1)$	2/27
7~18	$(\pm1,\pm1,0),(0,\pm1,\pm1),(\pm1,0,\pm1)$	1/54
19~26	$(\pm1,\pm1,\pm1)$	1/216

$\boldsymbol{S_h}$ is a diagonal matrix, which is expressed as follows:

$$\boldsymbol{S_h}=\mathrm{diag}(0,s_h,s_h,s_h,1.5,1.5,\ldots,1.5) \tag{18}$$

$$s_h = \frac{1}{\tau_h + 0.5} \tag{19}$$

$$M = \tau_h c_s^2 \delta_t \tag{20}$$

$$c_s = \frac{1}{\sqrt{3}} \tag{21}$$

$$\delta_t = \delta_x = 1 \tag{22}$$

$\boldsymbol{M}$ is the transformation moment, which will be shown at the end of this section.

Equation of continuity and Navier-Stokes equation are discretized using the velocity-based lattice Boltzmann method. The weighted MRT model is used to calculate the collision term.

$$f_i(x_\alpha + c_{i\alpha}\delta_t, t + \delta_t) = f_i(x_\alpha, t) - \boldsymbol{M^{-1}S_f M}\left(f_i(x_\alpha, t) - \overline{f_i^{eq}}(x_\alpha, t)\right) + F_i \tag{23}$$

$$\overline{f_i^{eq}} = f_i^{eq} - \frac{1}{2}F_i \tag{24}$$

Where f_i^{eq} is the equilibrium distribution function, F_i is the external force term, which is given as follows [6]:

$$f_i^{eq} = w_i\left[\frac{c_{i\alpha}u_\alpha}{c_s^2} + \frac{(c_{i\alpha}u_\alpha)^2}{2c_s^4} - \frac{u_\alpha^2}{2c_s^2}\right] \tag{25}$$

$$F_i = \delta_t w_i \frac{c_{i\alpha}F_\alpha}{\rho c_s^2} \tag{26}$$

F_α is a macroscopic external force term and is as follows:

$$F_\alpha = F_\alpha^s + F_\alpha^b + F_\alpha^p + F_\alpha^\mu \tag{27}$$

F_α^p is the pressure term and F_α^μ is the modified viscosity term, as follows:

$$F_\alpha^p = -\frac{\partial p}{\partial x_\alpha} \tag{28}$$

$$F_\alpha^\mu = -\frac{\mu}{(\tau_f + 0.5)\rho c_s^2 \delta_t}\left[\sum_i c_{i\alpha}c_{i\beta}\left(f_i - f_i^{eq}\right)\right]\frac{\partial \rho}{\partial x_\beta} \tag{29}$$

$\boldsymbol{S_f}$ is a diagonal matrix, expressed as follows:

$$\boldsymbol{S_f} = \text{diag}(1,1,1,1, s_f, s_f, s_f, s_f, 1,1, \ldots, 1) \tag{30}$$

$$s_f = \frac{1}{\tau_f + 0.5} \tag{31}$$

$$\mu = \tau_f \rho c_s^2 \delta_t \tag{32}$$

The first- and second-order differentials that appear in the formula are calculated as follows. θ is arbitrary physical quantity.

$$\frac{\partial \theta}{\partial x_\alpha} = \frac{1}{c_s^2 \delta_x}\sum_i c_{i\alpha} w_i \theta(x_i + c_{i\alpha}\delta_t, t) \tag{33}$$

$$\frac{\partial^2 \theta}{\partial x_\alpha^2} = \frac{2}{c_s^2 \delta_x^2}\sum_i w_i[\theta(x_i + c_{i\alpha}\delta_t, t) - \theta(x_i, t)] \tag{34}$$

To perform a fully explicit calculation, the pressure equation is solved using the following finite difference method.

$$p^*(x_\alpha, t+\delta_t) = p(x_\alpha, t) + \delta_t \rho c_s^2 \sum_i (f_i - f_i^{eq}) \tag{35}$$

In addition, to improve the stability near the interface, the pressure is calculated using a second-order spatial average.

$$p(x_\alpha, t+\delta_t) = \sum_i w_i p^*(x_\alpha + c_{i\alpha}\delta_t, t+\delta_t) \tag{36}$$

The transformation moment is defined by the following formula[7].

$$\boldsymbol{M} = [\boldsymbol{m_0}, \boldsymbol{m_1}, \dots, \boldsymbol{m_i}, \dots, \boldsymbol{m_{25}}, \boldsymbol{m_{26}}]^T \tag{37}$$

$$m_{0i} = 1 \tag{38}$$

$$m_{1i} = c_{ix} \tag{39}$$

$$m_{2i} = c_{iy} \tag{40}$$

$$m_{3i} = c_{iz} \tag{41}$$

$$m_{4i} = c_{ix}c_{iy} \tag{42}$$

$$m_{5i} = c_{iy}c_{iz} \tag{43}$$

$$m_{6i} = c_{iz}c_{ix} \tag{44}$$

$$m_{7i} = 3c_{ix}^2 - c_{i\alpha}^2 \tag{45}$$

$$m_{8i} = c_{iy}^2 - c_{iz}^2 \tag{46}$$

$$m_{9i} = c_{i\alpha}^2 - 1 \tag{47}$$

$$m_{10i} = 3c_{i\alpha}^2 c_{ix} - 5c_{ix} \tag{48}$$

$$m_{11i} = 3c_{i\alpha}^2 c_{iy} - 5c_{iy} \tag{49}$$

$$m_{12i} = 3c_{i\alpha}^2 c_{iz} - 5c_{iz} \tag{50}$$

$$m_{13i} = (c_{iy}c_{iy} - c_{iz}c_{iz})c_{ix} \tag{51}$$

$$m_{14i} = (c_{iz}c_{iz} - c_{ix}c_{ix})c_{iy} \tag{52}$$

$$m_{15i} = (c_{ix}c_{ix} - c_{iy}c_{iy})c_{iz} \tag{53}$$

$$m_{16i} = c_{ix}c_{iy}c_{iz} \tag{54}$$

$$m_{17i} = 1.5c_{i\alpha}^4 - 3.5(c_{i\alpha}^2 - 1) - 2.5 \tag{55}$$

$$m_{18i} = 3c_{i\alpha}^2(3c_{ix}^2 - c_{i\alpha}^2) - 4(3c_{ix}^2 - c_{i\alpha}^2) \tag{56}$$

$$m_{19i} = 3c_{i\alpha}^2\left(c_{iy}^2 - c_{iz}^2\right) - 4(c_{iy}^2 - c_{iz}^2) \tag{57}$$

$$m_{20i} = 3c_{ix}c_{iy}c_{i\alpha}^2 - 7c_{ix}c_{iy} \tag{58}$$

$$m_{21i} = 3c_{iy}c_{iz}c_{i\alpha}^2 - 7c_{iy}c_{iz} \tag{59}$$

$$m_{22i} = 3c_{iz}c_{ix}c_{i\alpha}^2 - 7c_{iz}c_{ix} \tag{60}$$

$$m_{23i} = 4.5c_{ix}c_{i\alpha}^4 - 5.5(3c_{i\alpha}^2c_{ix} - 5c_{ix}) - 14.5c_{ix} \tag{61}$$

$$m_{24i} = 4.5c_{iy}c_{i\alpha}^4 - 5.5\left(3c_{i\alpha}^2c_{iy} - 5c_{iy}\right) - 14.5c_{iy} \tag{62}$$

$$m_{25i} = 4.5c_{iz}c_{i\alpha}^4 - 5.5(3c_{i\alpha}^2c_{iz} - 5c_{iz}) - 14.5c_{iz} \tag{63}$$

$$m_{26i} = 4.5c_{i\alpha}^6 - 12(1.5c_{i\alpha}^4 - 3.5(c_{i\alpha}^2 - 1) - 2.5) - 25.5(c_{i\alpha}^2 - 1) - 14.5 \tag{64}$$

2.3. Ghost node method[8)]

In this study, the ghost node method is used to perform a numerical calculation of droplets bouncing. A ghost node layer is used on the collision surface between droplets, and Dirichlet boundary conditions are applied to it. In previous research [8)], the method was used in combination with the level set method, but the method is unsuitable during parallel calculation. Therefore, by combining it with the phase-field lattice Boltzmann method, high-speed calculations are achieved in the present study.

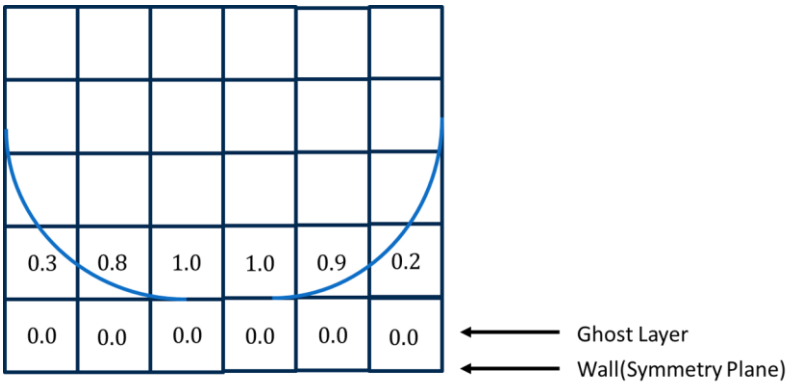

Figure 5. Illustration of ghost node method.

2.4. Energy calculation, radial expansion and algorithm

The energy conservation equation is shown below.

$$E_{total} = KE_{initial} + STE_{initial} = KE + STE + TDE \tag{65}$$

Where KE is kinetic energy, STE is surface tension energy, and TDE is dissipated energy.

In this study, the kinetic and surface tension energy are calculated. Note the kinetic energy is calculated for the entire region, while the formula for surface tension energy is calculated only for the interface region.

$$KE = \int_p \frac{1}{2}\rho V^2 dv_p \tag{66}$$

$$STE = \int \left(\beta\phi^2(1-\phi)^2 + \frac{\kappa}{2}\left|\frac{\partial\phi}{\partial x}\right|^2\right) dv_p \tag{67}$$

Radial Expansion represents the expansion and contraction in the radial direction of the droplet.

$$RE = \frac{D}{D_0} \tag{68}$$

The algorithm is as follows:
Step 1. Initial conditions
Step 2. Translation process calculation
Step 3. Boundary conditions
Step 4. Calculation of macroscopic physical quantities
Step 5. Application of the ghost node method
Step 6. Pressure calculation
Step 7. Collision process calculation
Step 8. Outputs
Step 9. Return to Step 2

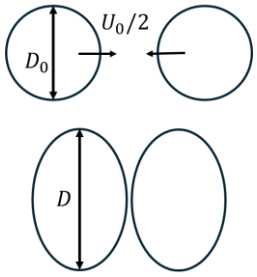

Figure 6. Illustration of Radial Expansion. (above: initial condition, below: Calculation in progress.)

3. Numerical calculation results

3.1. Calculation conditions

The calculation conditions are listed in Tables 2 and 3. The following values are used for the Reynolds number and Weber number for comparison with the experimental results of previous research. The calculation was performed up to 2.0ms in dimensional time.

Table 2. Calculation condition[9)]

Parameter	Case1	Case2
Re	111	55.27
We	9.33	2.27

Table 3. Common parameters.

Parameter	Value
Grid	32
Mach number	$0.01\sqrt{3}$
mobility	0.05
Interface width	5
Impact parameter	0.0
Density ratio	760
Viscosity ratio	118.75

The Reynolds number and Weber number are defined as follows:

$$Re = \frac{U_0 \rho D}{\mu_h} \tag{69}$$

$$We = \frac{\rho_h D U_0^2}{\sigma} \tag{70}$$

3.2. Results

First, the results of Case 1 are presented. Figure 7 shows the time series of droplet collisions. Comparing the simulation results obtained in this analysis with the experimental results[9)], we can confirm that the shapes of Cases 1 is roughly consistent. It can also be seen that there are gaps between the droplets. This is because the ghost node method requires ghost layer on the collision surface.

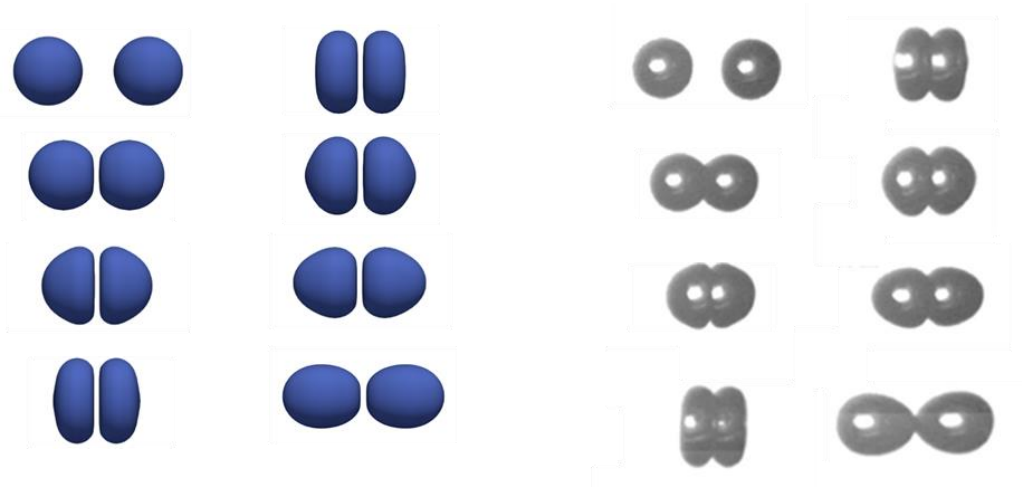

Figure 7. Result of Case1 (Left: Numerical result, Right: Experimental result). (t = 0.0, 0.20, 0.35, 0.49, 0.61, 0.70, 0.80, 0.99 ms.) [9]

The volume conservation was less than 0.02% in both cases, making use of the advantages of the lattice Boltzmann method. You can also see that the graph of volume change is oscillating. This is because the pressure equation is solved explicit method. Figures 8 and 9 show the results for the maximum droplet radius. First, the droplet is stretched in the radial direction due to collision. Then, it can be confirmed that it repeatedly expands and contracts due to recoil.

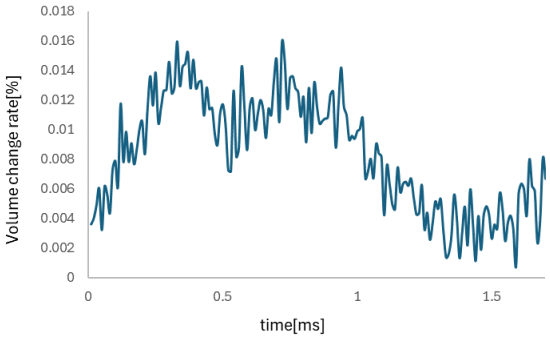

Figure 8. Volume change rate graph.

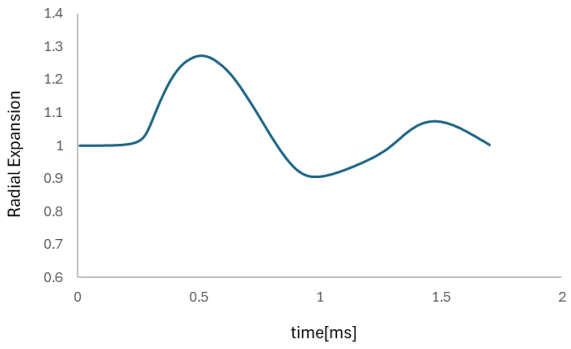

Figure 9. Radial expansion graph.

Figure 10 shows the changes in the kinetic energy and surface tension energy over time. As the droplet collides, the kinetic energy decreases and, the surface tension energy increases. After that, the kinetic energy increases again, and the surface tension energy decreases. We can also see that the graph of STE change is oscillating. This is because the pressure equation is solved explicit method. In addition, since the calculation of STE is greatly influenced by the interface shape, we believe that even slight interface vibrations are reflected in the STE.

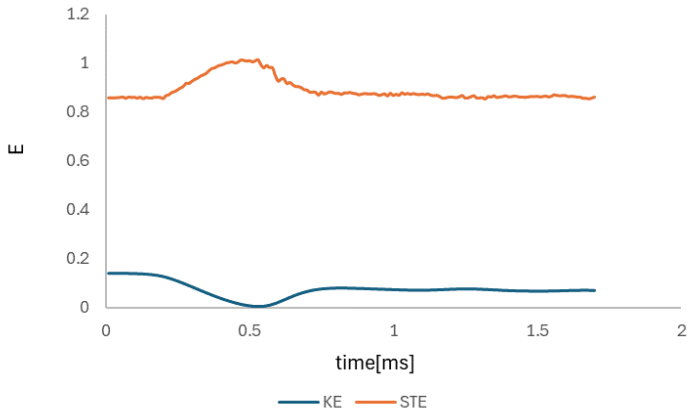

Figure 10. Energy graph.

Next, the results of Case 2 are presented. As in Case 1, Comparing the simulation results obtained in this analysis with the experimental results[9], we can confirm that the shapes of Cases 1 is roughly consistent.

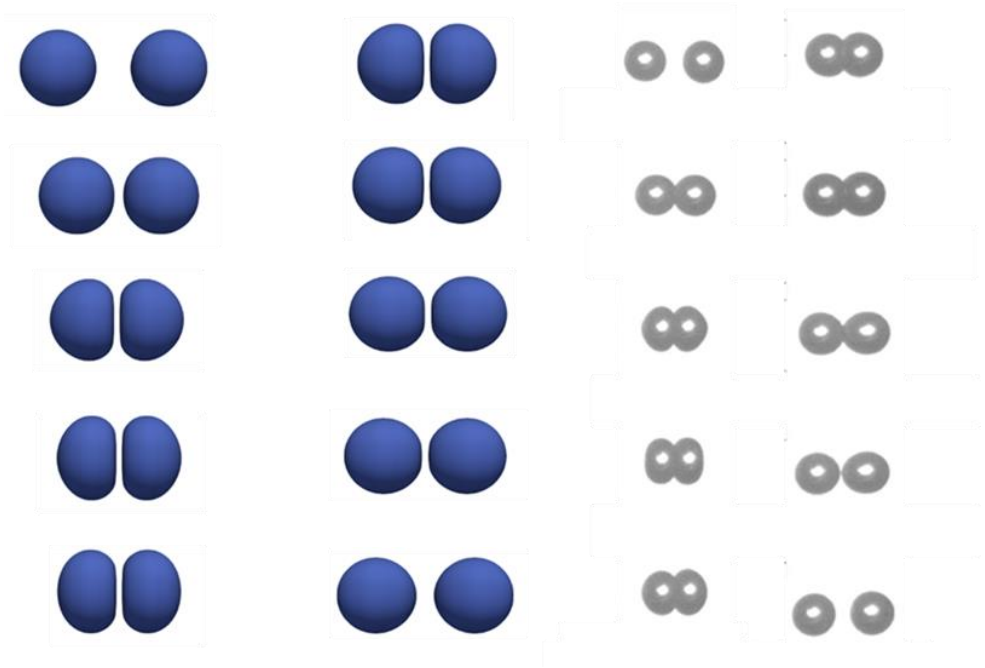

Figure 11. Result of Case2 (Left: Numerical result, Right: Experimental result). (t = 0.0, 0.30, 0.60, 0.70, 0.90, 1.05, 1.15, 1.25, 1.30, 1.50 ms.)[9]

The volume conservation was less than 0.02% in both cases, making use of the advantages of the lattice Boltzmann method. Figures 12 and 13 show the results for the maximum droplet radius. First, the droplet is stretched in the radial direction due to collision as in Case 1. Then, it can be confirmed that it repeatedly expands and contracts due to recoil. On the other hand, the droplet bound time is slower than in Case 1 because the Weber number is smaller.

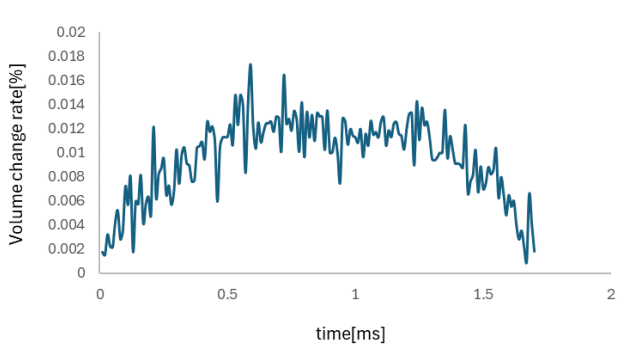

Figure 12. Volume change rate graph.

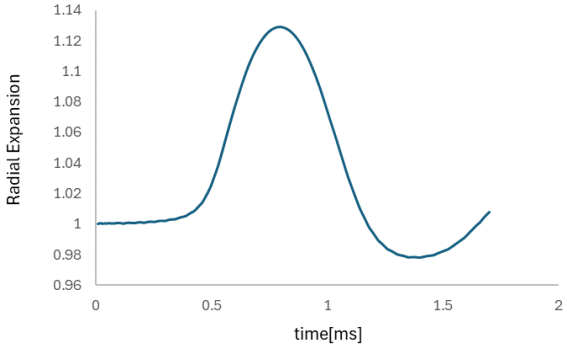

Figure 13. Radial expansion graph.

Figures 14 and 15 show the changes in the kinetic energy and surface tension energy over time. As the droplet collides, the kinetic energy decreases, and the surface tension energy increases as in Case 1. On the other hand, since the Weber number is smaller than in Case 1, the ratio of kinetic energy to total energy is smaller. This trend is consistent with previous research[9], and it demonstrates the validity of the proposed method.

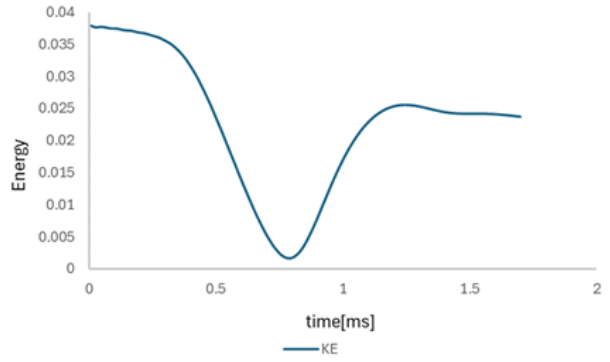

Figure 14. Kinetic energy graph.

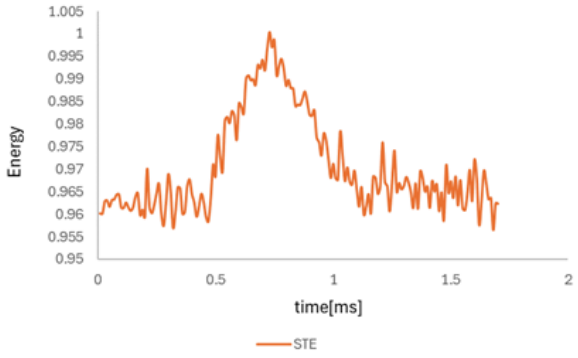

Figure 15. Surface tension energy graph.

4. Conclusion

The purpose of this study was to use the proposed method to perform numerical calculations of the collision phenomenon related to droplet rebound and to verify its validity. The proposed method is a coupling of the phase-field lattice Boltzmann method, which is suitable for parallel calculations, and the ghost node method, which has low implementation costs. Calculations were performed and compared with previous studies[9], proving the validity of the proposed method. It was also found that the advantages of the lattice Boltzmann method, such as good volume conservation and suitability for parallel calculations using GPUs, were able to be utilized.

In future, we plan to expand the proposed method to calculations when droplets are misaligned, i.e., collision parameter I is other than 0.

References

1) N. Ashgriz and J. Y. Poo: Coalescence and separation in binary collisions of liquid drops. J. Fluid Mech. vol.221 (1990), pp. 183-204, DOI: 10.1017/S0022112090003536

2) P. R. Brazier-Smith, S. G. Jennings and J. Latham: The interaction of falling water drops: coalescence. Proceedings of the Royal Society of London. A. Mathematical, Physical and Engineering Sciences (1972), pp. 393-408, DOI: https://doi.org/10.1098/rspa.1972.0016

3) N. Nikolopoulos, and G. Bergeles: The effect of gas and liquid properties and droplet size ratio on the central collision between two unequal-size droplets in the reflexive regime. International journal of heat and mass transfer (2011), 54(1-3), 678-691., DOI: https://doi.org/10.1016/j.ijheatmasstransfer.2010.09.002
4) Y. Pan and K. Suga: Numerical simulation of binary liquid droplet collision. Physics of Fluids 17.8 (2005), DOI: https://doi.org/10.1063/1.2009527
5) F. Ren, B. Song, M. C. Sukop and H. Hu: Improved lattice Boltzmann modeling of binary flow based on the conservative Allen-Cahn equation. Physical Review E (2016), 94(2), 023311, DOI: https://doi.org/10.1103/PhysRevE.94.023311
6) Y. P. Sitompul and T. Aoki: A filtered cumulant lattice Boltzmann method for violent two-phase flows. Journal of Computational Physics (2019), 390, 93-120, DOI: https://doi.org/10.1016/j.jcp.2019.04.019
7) A. Fakhari, D. Bolster and L. S. Luo: A weighted multiple-relaxation-time lattice Boltzmann method for multiphase flows and its application to partial coalescence cascades. Journal of Computational Physics 341.15 (2017), DOI: https://doi.org/10.1016/j.jcp.2017.03.062
8) A. Amani, N. Balcazar, E. Gutierrez and A. Oliva: Numerical study of binary droplets collision in the main collision regimes. Chemical Engineering Journal 370 (2019), 477-498, DOI: https://doi.org/10.1016/j.cej.2019.03.188
9) K. L. Pan, C. K. Law and B. Zhou: Experimental and mechanistic description of merging and bouncing in head-on binary droplet collision. Journal of Applied Physics 103.6 (2008), DOI: https://doi.org/10.1063/1.2841055